Lyapunov-Designed Super-Twisting Sliding Mode Control for Wind Energy Conversion Optimization

C. Evangelista, P. Puleston, F. Valenciaga, and L. M. Fridman

Abstract—This work explores an adaptive second-order sliding mode control strategy to maximize the energy production of a wind energy conversion system (WECS) simultaneously reducing the mechanical stress on the shaft. Such strategy successfully deals with the random nature of wind speed, the intrinsic nonlinear behavior of the WECS, and the presence of model uncertainties and external perturbations acting on the system. The synthesized adaptive controller is designed from a modified version of the super-twisting (ST) algorithm with variable gains. The suitability of the proposed strategy is proved by extensive computer-aided simulations employing a comprehensive model of the system emulating realistic conditions of operation, i.e., considering variations in the parameters and including external disturbances. Additionally, a second controller based on the traditional ST algorithm is also designed and simulated. Results are presented and discussed in order to establish a comparison framework.

Index Terms—Sliding mode control, super-twisting (ST), wind power generation.

I. INTRODUCTION

IT IS well known that, due to several reasons, worldwide attention has turned to renewable energy sources, among which wind represents one of the most interesting options. Its exploitation has been one of the most dynamically growing for the last years. By the end of 2010, wind turbines were generating 2.5% of the world electricity consumption, and the global wind installed capacity exceeded 197 GW [1], [2].

This growing trend must be accompanied by continuous technological development and optimization, leading to better options concerning reductions in costs, integration to the grid, and improvements regarding turbine performance and reliability in the electricity delivery. Among the main research subjects in the wind energy field, there is the exploration of novel control strategies, which must cope with the exacting characteristics presented by wind energy conversion system (WECS) such as the nonlinear behavior of the system, usual uncertainties in both the aerodynamic and the electrical models, and the presence of external perturbations and the random variability of the wind.

In this context, it results of interest to explore the use of second-order sliding mode (SOSM) algorithms, which are an excellent option to control nonlinear uncertain systems operating in perturbed environments [3]. Roughly speaking, SOSM techniques consist of zeroing the sliding variable σ and its first time derivative $\dot{\sigma}$ in finite time, through a continuous control $u(t)$ acting discontinuously on its second time derivative $\ddot{\sigma}$, reducing strongly the chattering phenomenon. They result in controllers with several attractive characteristics [4]–[16].

1) Robustness with respect to various internal and external disturbances and model uncertainties, allowing accurate regulation and tracking.
2) Finite-time convergence.
3) Reduction of mechanical stresses and chattering (i.e., high-frequency vibrations of the controlled system), compared to standard sliding mode strategies, given that the applied control actions are continuous.
4) Relatively simple control laws, which entail low real-time computational burden.
5) The design procedure is capable of dealing with nonlinear descriptions of the system, and therefore, wider ranges of operation are attained, in comparison to design techniques based on model linearization.

This work presents a controller based on the super-twisting (ST) algorithm with variable gains proposed by Dávila *et al.* [17], using Lyapunov techniques. In particular, it has been applied and developed to control a grid-connected variable-speed WECS topology with slip power recovery, which can be electronically controlled. Its variable speed feature allows to seek power conversion maximization in the zone of operation known as partial load zone, where the wind speed is below the rated one of the turbine. The followed control objective was to optimize its power conversion efficiency, reducing mechanical fatigue and attenuating the output chattering.

Additionally, a nonadaptive SOSM controller is designed, in order to both assess its applicability to the studied WECS and to compare its performance with the adaptive-gain proposal. Suitable candidates could be a classic ST structure or other constant-gain SOSM algorithms (e.g., twisting or suboptimal) with the incorporation of an integrator to increase the relative degree. The ST algorithm, originally presented by Levant [11], has been preferred given that it can be directly applied to systems of relative degree 1 (as the considered WECS), and moreover, it does not require information of $\dot{\sigma}$ for its implementation. For comparative reasons, the fixed-gain ST controller has been tuned following the development presented by Moreno and Osorio [18] since the design method is based on Lyapunov
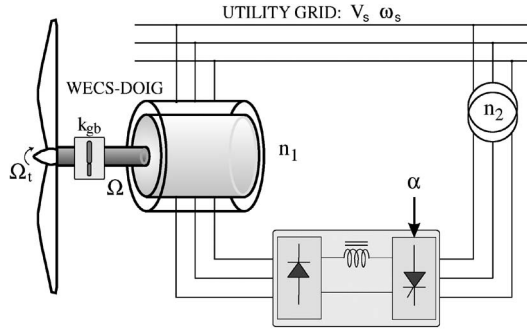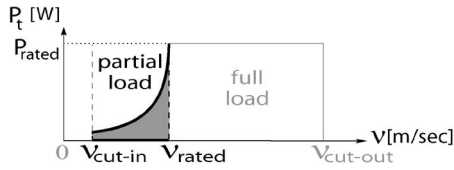
Fig. 1. WECS-DOIG with SKD.

Fig. 2. Wind turbine operation zone.

and is analogous to the one proposed for the variable-gain ST algorithm.

This paper is organized as follows. The WECS and the control objective are briefly explained in Section II. The control design is described in Section III, including the development of the variable-gain and the fixed-gain ST controllers in Sections III-A and III-B, respectively. Simulation results are shown in Section IV, where the two strategies are evaluated. Finally, conclusions are presented in Section V.

II. WECS DESCRIPTION

Grid-connected WECS based on a double-output induction generator (DOIG) with slip power recovery is considered. Such variable-speed configuration can operate at different speeds but generates electricity at the constant frequency and voltage fixed by the grid and, adequately controlled, allows power conversion maximization and mechanical stress alleviation. In particular, in this paper, a simple topology has been selected as a case of study, namely, one that uses a static Kramer drive (SKD) as slip power recovery drive. A schematic diagram of this configuration is shown in Fig. 1.

As it can be observed, both stator and rotor circuits provide power to the grid, making the system capable of generation above its rated power. While the former is directly delivered to the grid, the latter is partially recovered through an electronic converter, which processes only the recovered power. This converter consists of an uncontrolled bridge rectifier, a smoothing reactor, and a line-commutated inverter, whose firing angle α can be modified to control the generator torque and, hence, the system operation speed and the operation point [19]–[21].

Starting the description of the WECS with the aerodynamic subsystem, it should be mentioned that the present work focuses on the partial load zone of operation, within which the control objective is to extract the maximum power from the wind. As it can be seen in Fig. 2, the partial load zone is the operation zone between the cut-in (when the wind energy is not sufficient to
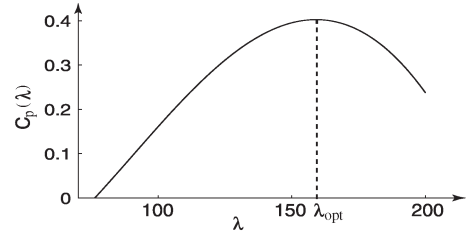

Fig. 3. Power coefficient versus tip speed ratio.

move on the turbine) and the rated wind speed [22]. Operation above the rated wind speed is not considered here, and the existence of a power-limiting mechanism has been assumed (possibly by actively or passively changing its aerodynamic characteristics).

For the subsequent analysis, a rigid drive train has been assumed, and for mathematical simplicity, every turbine variable in this paper has been rendered at the fast shaft or generator side through the transmission ratio k_{gb} of the gear box (see Appendix A).

The mechanical power that a real turbine can capture is only a fraction of the available power in the wind, and it can be written as [23]

$$P_t = 0.5\pi\rho R^2 C_p(\lambda)\nu^3 \tag{1}$$

where ν is the wind speed, ρ is the air density, R is the blade length, and $C_p(\lambda)$ is the conversion efficiency or power coefficient of the WECS. This coefficient is a nonlinear function of the called tip speed ratio $\lambda = R\Omega/\nu$, with Ω being the mechanical rotation speed, and depends on the shape and geometrical dimensions of the rotor, presenting for a turbine with fixed pitch a single maximum.

Therefore, power efficiency maximization is obtained if the tip speed ratio is kept equal to λ_{opt}, which can be accomplished by controlling the system speed operation to track the variable optimum reference given by [22], [23]

$$\Omega_{\mathrm{ref}} = \frac{\lambda_{\mathrm{opt}}\nu}{R}. \tag{2}$$

The power coefficient curve for the three-bladed turbine used in this work, modeled as $C_p(\lambda) = \sum_{i=0}^{3} c_i\lambda^i$, is depicted in Fig. 3.

An expression for the turbine torque T_t is obtained from the quotient P_t/Ω, and defining the torque coefficient of the turbine as $C_t(\lambda) = C_p(\lambda)/\lambda$, it can be written as

$$T_t = 0.5\pi\rho R^3 C_t(\lambda)\nu^2. \tag{3}$$

Regarding the electromechanical subsystem of the WECS, it is reasonable to assume that the electrical dynamics are considerably faster than the mechanical ones. Therefore, a reduced-order model considering the dominant dynamics is used in this work for the controller design. Then, the nonlinear dynamic equation of the system can be straightforwardly obtained by applying Newton's second law, including a term $g(\cdot)$ to consider
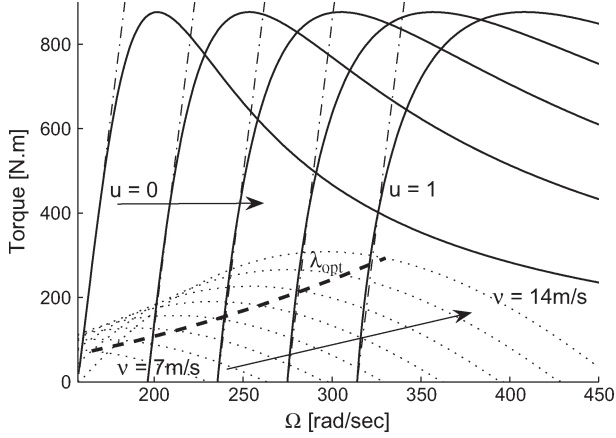
Fig. 4. (Solid lines) Torque versus rotational speed characteristics of the DOIG. (Dotted lines) Wind turbine characteristic for different wind speeds. (Dash-dotted lines) Affine approximation to DOIG characteristic. (Bold dashed line) Maximum power generation locus.

friction, uncertainties, and other disturbances, and it can be stated as

$$\dot{\Omega} = \frac{1}{J} \left(T_t \left(\Omega, \nu(t) \right) + T_e(\Omega, u) \right) + g(\Omega, t) \qquad (4)$$

where J is the inertia of the combined rotating parts, T_e is the electrical resistant torque of the generator ($T_e < 0$ as generator), and u is the control action. Although the generator torque is physically modified by the controlled firing angle α, in this design framework, the variable $u = |\cos(\alpha)|$ is used as the control action for simplicity's sake. In this context, the expression of the generator torque is given by [24]

$$T_e(\Omega, u, t) = \frac{3V_s'^2 s R_{eq}}{\Omega_s \left[(sR_s' + R_{eq})^2 + (s\omega_s L)^2 \right]} \qquad (5)$$

where

$$R_{eq} = \frac{s}{s^2 - n^2 u^2} \left[sR_b + n^2 u^2 R_s' \right.$$
$$\left. - nu \sqrt{\left| (R_b + sR_s')^2 + \omega_s^2 L^2 (s^2 - n^2 u^2) \right|} \right]$$

where $R_b = R_r + 0.55 R_f$ and $L = L_s' + L_r$. R_s, R_r, and R_f are the resistance of the stator, rotor, and dc link, respectively, L_s and L_r are the leakage inductances of stator and rotor windings, Ω_s and ω_s are the mechanical and electrical synchronous speeds, $s = 1 - \Omega/\Omega_s$ is the generator slip, V_s is the stator voltage, and $n = n_1/n_2$, with n_1 and n_2 being the turns ratios of the generator and the step-down transformer, respectively. Note that a single quotation mark applied to a stator variable indicates that it has been referred to the rotor windings by n_1.

The torque characteristics T_t and $-T_e$ are schematically depicted in Fig. 4, in the $T - \Omega$ plane. The curves in solid lines show the variation of $-T_e$ with Ω for some values of the control action u, while the variation of T_t is depicted in dotted lines for several wind speeds. The geometric locus corresponding to the points of maximum power generation is also presented in the picture in bold dashed line.

III. CONTROLLER DESIGN

The expression of the generator torque can be rewritten as

$$T_e(\Omega, u, t) = \frac{3V_s'^2 n}{\Omega_s R_b} u + \frac{3V_s'^2}{\Omega_s R_b} \left(1 - \frac{\Omega}{\Omega_s} \right) + \Delta T_e(\Omega, t)$$
$$= B_1 u + T_{e_1}(\Omega) + \Delta T_e(\Omega, t) \qquad (6)$$

where the two first terms correspond to an affine in the control approximation of the generator torque and the third term ΔT_e takes into account the remaining differences.

In the zone of operation, where the torque keeps below the rated one, the term $\Delta T_e(\cdot)$ is considerably small, and consequently, the affine description results a good approximation for T_e (see characteristic in dash-dotted lines in Fig. 4).

Replacing (6) into (4), it results in

$$\dot{\Omega} = \frac{B_1}{J} u + \frac{T_t(\Omega, \nu) + T_{e_1}(\Omega)}{J} + g(\Omega, t) + \frac{\Delta T_e(\Omega, t)}{J}. \qquad (7)$$

At this point, to accomplish the speed reference tracking, the sliding variable is chosen as

$$\sigma = \frac{J}{B_1} \left(\Omega - \Omega_{ref}(t) \right). \qquad (8)$$

In this way, the 2-sliding condition $\dot{\sigma} = \sigma = 0$ guarantees the main control objective $\Omega = \Omega_{ref}$. At the same time, the inclusion of the constant factor J/B_1 allows to express the sliding dynamics in the regular form using (2), (7), and (8)

$$\dot{\sigma} = \frac{J}{B_1} \dot{\Omega} - \frac{J\lambda_{opt}}{B_1 R} \dot{\nu} = u + F(\sigma, t) + G(\sigma, t) \qquad (9)$$

$$F(\sigma, t) = \frac{1}{B_1} \left(T_t(\Omega, \nu) + T_{e_1}(\Omega) - \frac{J\lambda_{opt}}{R} \dot{\nu} \right) \qquad (10)$$

$$G(\sigma, t) = \frac{1}{B_1} \left(g(\Omega, t) + \Delta T_e(\Omega, t) + J\Delta\Omega_{ref}(t) \right) \qquad (11)$$

where $\Omega = (B_1/J)\sigma + (\lambda_{opt}/R)\nu$ and $\Delta\Omega_{ref}(t)$ considers the errors in the determination of the reference. Function F represents the nominal or undisturbed design model, and function G takes into account measurement and modeling errors, uncertainties in the parameters, and external disturbances.

A two-component control action is proposed as $u = u_{eq} + \tilde{u}$, where u_{eq} is the equivalent control for system (7) and $\tilde{u}$ is designed using a modified version of the ST algorithm.

The expression of u_{eq} is computed from the undisturbed system (9) (i.e., $G(\sigma, t) = 0$). It is obtained by solving for u in the algebraic equation $\dot{\sigma} = 0$, on the sliding surface (i.e. with $\sigma = 0$) [25]. Writing $k_o = \lambda_{opt}/R$, the expression for u_{eq} is

$$u_{eq} = -F(0, t) = \frac{Jk_o\dot{\nu} - T_t(k_o\nu, \nu) - T_{e_1}(k_o\nu)}{B_1}. \qquad (12)$$

Using this formula, (9) can be written as

$$\dot{\sigma} = u_{eq} + \tilde{u} + F(\sigma, t) + G(\sigma, t) = \tilde{u} + \tilde{G}(\sigma, t) \qquad (13)$$

where $\tilde{G}(\sigma,t)=F(\sigma,t)-F(0,t)+G(\sigma,t)$. This function can be divided into two terms such as $\tilde{G}(\sigma,t)=\tilde{G}_1(\sigma,t)+\tilde{G}_2(t)$

$$\tilde{G}_2(t) = \tilde{G}(0,t) \tag{14}$$

$$\tilde{G}_1(\sigma,t) = \tilde{G}(\sigma,t) - \tilde{G}(0,t). \tag{15}$$

The design of $\tilde{u}$ is based on certain bounding functions which must be found for $\tilde{G}_1(\sigma,t)$ and the time derivative of $\tilde{G}_2(t)$.

In the following sections, two designs are developed for this term. In the main proposal, $\tilde{u}$ has variable gains and is a variation of the Lyapunov-based design presented in [17]. Its adaptive characteristic is intended to be beneficial regarding output chattering and mechanical efforts applied to the shaft. As a second case of study, the Lyapunov-based standard ST algorithm proposed in [18] is applied to this control problem.

A. Variable-Gain ST

The variable-gain ST control action term $\tilde{u}$ has the form

$$\tilde{u} = -k_1(\sigma,t)\phi_1(\sigma) - \int_0^t k_2(\sigma,\tau)\phi_2(\sigma)d\tau \tag{16}$$

$$\phi_1(\sigma) = k_c|\sigma|^{\frac{1}{2}}\text{sign}(\sigma), \qquad k_c > 0 \tag{17}$$

$$\phi_2(\sigma) = \phi_1'(\sigma)\phi_1(\sigma) = \frac{k_c^2}{2}\text{sign}(\sigma). \tag{18}$$

The constant k_c is not present in the original algorithm. It has been considered here as an additional tuning parameter to allow a better behavior of the controlled system with respect to chattering. Then, defining $z_1 = \sigma$ and $z_2 = -\int_0^t k_2(\sigma,t)\phi_2(\sigma)dt + \tilde{G}_2(t)$ as the new states, the closed-loop system dynamics for (13) with the variable-gain ST control law given in (16) can be written as

$$\begin{cases} \dot{z}_1 = -k_1(z_1,t)\phi_1(z_1) + z_2 + \tilde{G}_1(z_1,t) \\ \dot{z}_2 = -k_2(z_1,t)\phi_2(z_1) + \frac{d}{dt}\tilde{G}_2(t). \end{cases} \tag{19}$$

A Lyapunov function can be found for this system so that, if the components of $\tilde{G}$ can be bounded such that

$$\left|\tilde{G}_1(z_1,t)\right| \le \varrho_1(z_1,t)\left|\phi_1(z_1)\right| = \varrho_1(z_1,t)k_c|z_1|^{\frac{1}{2}} \tag{20}$$

$$\left|\frac{d}{dt}\tilde{G}_2(t)\right| \le \varrho_2(z_1,t)\left|\phi_2(z_1)\right| = \varrho_2(z_1,t)\frac{k_c^2}{2} \tag{21}$$

with some known positive functions $\varrho_1(z_1,t)$ and $\varrho_2(z_1,t)$ and for four constants $\epsilon > 0, p_1 > 0, p_2 < -\epsilon,$ and $p_3 > 0$ verifying $p_1 p_3 > p_2^2$, the varying gains of $\tilde{u}$ are selected as

$$k_1(z_1,t) = \frac{p_3}{p_1 p_3 - p_2^2}\left(\frac{(p_3\varrho_2 - p_2\varrho_1)^2}{-4(p_2 + \epsilon)} + p_1\varrho_1 - p_2\varrho_2\right.$$
$$\left. - \frac{p_1 p_2}{p_3} + \epsilon\right) + \delta, \quad \delta > 0 \tag{22}$$

$$k_2(z_1,t) = \frac{p_1}{p_3} - \frac{p_2}{p_3}k_1(z_1,t) \tag{23}$$

with δ being small, then the trajectories of the controlled system (19) converge to the origin in finite time despite the perturbations.

This can be proved using the following Lyapunov function:

$$V(z) = \zeta^T P\zeta \tag{24}$$

with $\zeta^T = [\phi_1(z_1), z_2] = [k_c|z_1|^{1/2}\text{sign}(z_1), z_2]$ and

$$P = \begin{bmatrix} p_1 & p_2 \\ p_2 & p_3 \end{bmatrix} = P^T > 0.$$

Then, a procedure similar to the one developed in the general proof in [17] is followed. Given that conditions (20)–(23) are verified for the WECS under study, it can be shown that the time derivative of the Lyapunov function is bounded by

$$\dot{V} \le -\epsilon\phi_1'(z_1)\zeta^T\zeta = -\frac{\epsilon k_c}{2|z_1|^{1/2}}\|\zeta\|_2^2 \tag{25}$$

where $\|\zeta\|_2^2 = k_c^2|z_1| + z_2^2$ is the Euclidean norm. Hence, from the standard inequality for quadratic forms

$$\lambda_{\text{Pm}}\|\zeta\|_2^2 \le \zeta^T P\zeta = V(z) \le \lambda_{\text{PM}}\|\zeta\|_2^2 \tag{26}$$

where λ_{Pm} and λ_{PM} are the minimum and the maximum eigenvalues of P, it stands that

$$V^{\frac{1}{2}} \ge \lambda_{\text{Pm}}^{\frac{1}{2}}\|\zeta\|_2 \ge \lambda_{\text{Pm}}^{\frac{1}{2}}k_c|z_1|^{\frac{1}{2}}. \tag{27}$$

Moreover, finally, from (25), (26), and (27)

$$\dot{V} \le -\frac{\epsilon k_c}{2|z_1|^{\frac{1}{2}}}\frac{V}{\lambda_{\text{PM}}} \le -\frac{\epsilon k_c^2\lambda_{\text{Pm}}^{\frac{1}{2}}}{2\lambda_{\text{PM}}}V^{\frac{1}{2}} = -\gamma V^{\frac{1}{2}} \tag{28}$$

with $\gamma = (\epsilon k_c^2\lambda_{\text{Pm}}^{1/2}/2\lambda_{\text{PM}}) > 0$, which shows that $V(z)$ is a strong Lyapunov function. Consequently, by the comparison principle [26], $V(z)$ and, therefore, the trajectories of (19) converge to zero in finite time.

The expression of $\tilde{G}(z_1,t)$ for the WECS under study is given in Appendix B. It has been computed by the propagation of error of (9), considering uncertainties in nominal parameters, variable measurement errors, and the addition of disturbances. In this case of study, the parameters taken into account as sources of errors and perturbations were the electrical resistances ($\pm 20\%$ of their nominal values), the grid nominal voltage ($\pm 15\%$ of its nominal value), bounded wind speed measurement errors, and the coefficients of the polynomial which describes the torque coefficient of the turbine C_t ($\pm 10\%$ of their nominal values). As a strong disturbance, an unmodeled friction torque has been included, computed as a quadratic function of the rotational speed with the addition of a random varying independent term (up to $\pm 10\%$ of the friction), generated as band-limited white noise.

Following the described procedure, analytical expressions have been found for the bounding functions

$$\varrho_1(z_1,t) = \frac{1}{k_c}|z_1|^{\frac{1}{2}}\left(A_1 + A_2|z_1| + A_3 z_1^2\right) \tag{29}$$

$$\varrho_2(z_1,t) = \frac{A_0}{k_c^2} \tag{30}$$

where the values for constants A_0–A_3 are given in Appendix A. The final tuning was aided by simulation tests, selecting the

values for the remaining control design parameters according to the objective of reducing mechanical loads and output chattering in the controlled system. The chosen values for k_c, p_1, p_2, p_3, ϵ, and δ to compute $k_1(z_1, t)$ and $k_2(z_1, t)$ according to (22) and (23) are also in Appendix A.

B. Fixed-Gain ST

In this case, the control action expression for the term $\tilde{u}$ in (13) is similar to (16), but using fixed gains

$$\tilde{u} = -k_1 \phi_1(\sigma) - k_2 \int_0^t \phi_2(\sigma) d\tau \quad (31)$$

where $\phi_1(\sigma)$ and $\phi_2(\sigma)$ are the ones in (17) and (18) with $k_c = 1$

$$\phi_1(\sigma) = |\sigma|^{\frac{1}{2}} \text{sign}(\sigma) \quad (32)$$

$$\phi_2(\sigma) = \phi_1'(\sigma) \phi_1(\sigma) = \frac{1}{2} \text{sign}(\sigma). \quad (33)$$

Proceeding similarly to the variable-gain case, new states $z_1 = \sigma$ and $z_2 = -k_2 \int_0^t \phi_2(\sigma) dt + \tilde{G}_2(t)$ are defined. Then, bounding the components of $\tilde{G}$ as

$$\left| \tilde{G}_1(z_1, t) \right| \leq \delta_1 |\phi_1(z_1)| = \delta_1 |z_1|^{\frac{1}{2}} \quad (34)$$

$$\left| \frac{d}{dt} \tilde{G}_2(t) \right| \leq \delta_2 \quad (35)$$

with δ_1 and δ_2 positive constants, the proposed Lyapunov function (24) guarantees that the trajectories of the controlled WECS converge to the origin in finite time, having chosen the fixed gains to verify [18]

$$k_1 > 2\delta_1 \quad (36)$$

$$k_2 > k_1 \frac{5\delta_1 + 6\delta_2 + 4(\delta_1 + \delta_2/k_1)^2}{2(k_1 - 2\delta_1)}. \quad (37)$$

It follows from (20) and (21) and (34) and (35) that δ_1 and δ_2 for the WECS under study can be obtained bounding the functions $\varrho_1(z_1, t)$ and $\varrho_2(z_1, t)$ in (29) and (30), found for the calculation of the variable gains. The constants δ_1 and δ_2 must satisfy

$$\delta_1 \geq |z_1|^{\frac{1}{2}} \left(A_1 + A_2 |z_1| + A_3 z_1^2 \right) \quad (38)$$

$$\delta_2 \geq \frac{A_0}{2}. \quad (39)$$

Clearly, a global use of this algorithm would not be convenient. Therefore, it is necessary to establish a maximum for $z_1 = \sigma = (J/B_1)(\Omega - \Omega_{\text{ref}}(t))$ to determine the value of δ_1. In this case of study, this maximum was derived assuming values for Ω within the range $|\Omega - \Omega_{\text{ref}}(t)| = 5$ rad/s, and the final selection was aided by simulation tests, considering the same disturbances and parameter uncertainties described in Section III-A. The chosen values for δ_1, δ_2 and the gains k_1 and k_2 can be found in Appendix A.
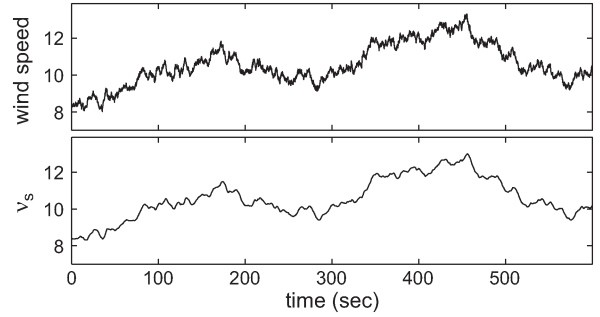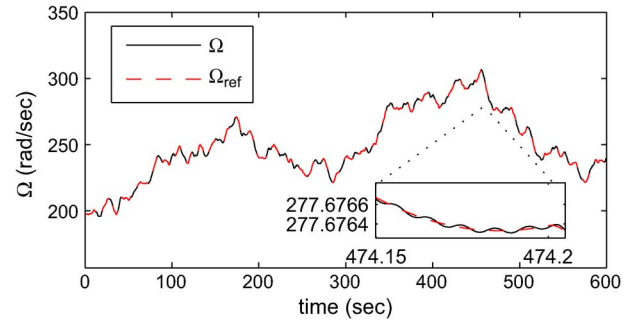

Fig. 5. Wind speed profile and quasi-steady term.

Fig. 6. Rotational speed and speed reference.

IV. SIMULATION RESULTS

To assess the designed controllers under realistic conditions, several tests were conducted using a full-order model of the WECS including both the mechanical and the electric dynamics, together with uncertainties and disturbances. The fifth-order set of differential equations used in these simulations to model the WECS based on DOIG-SKD is detailed in Appendix C [27].

The performance of the controlled system is shown herein through a representative example. For the simulations, the system is set to operate in the partial load zone, incorporating disturbances and parameter variations within the ranges summarized in Section III-A. The 10-min wind profile used in the presented simulations can be seen in the upper box of Fig. 5, modeled by adding a high-frequency turbulent term to the quasi-steady term ν_s, which is the one that provides useful work and generates power, and was used for the control design and tracking (see bottom box of Fig. 5) [28]. The bounds of ν_s considered for the design are in Appendix A.

A. Variable-Gain ST

The evolution of the rotational speed and the reference Ω_{ref} is depicted in Fig. 6. After a brief reaching time, the difference between the two variables is negligible, as it can be appreciated in the zoom box. The sliding variable is presented in Fig. 7, where the practical fulfillment of condition $\sigma = (J/B_1)(\Omega - \Omega_{\text{ref}}(t)) = 0$ can be observed, and it can be inferred from the comparison of both speed curves in Fig. 6. Note that the system operates in sliding exhibiting practically no chattering and proving the robustness of the controller in the presence of the aforementioned disturbances.
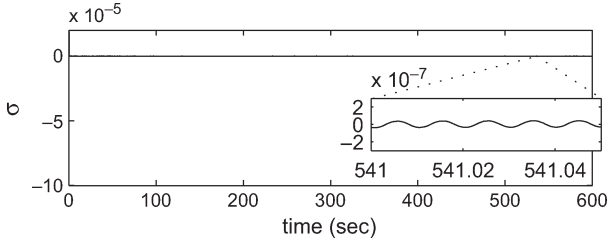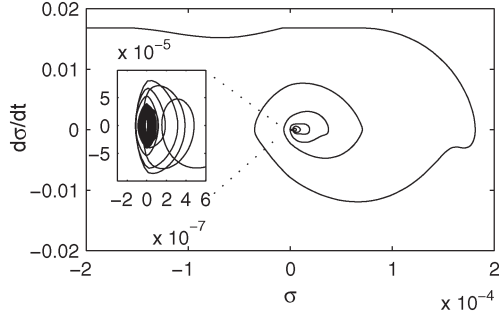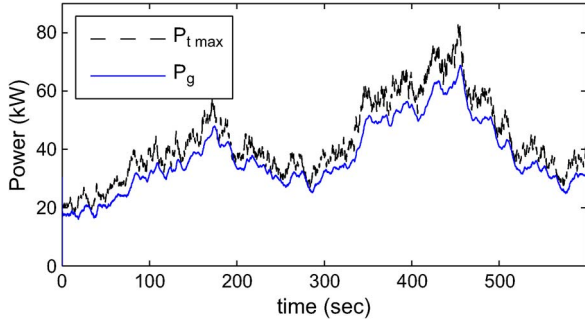
Fig. 7. Sliding variable $\sigma(t)$.

Fig. 8. $\sigma - \dot{\sigma}$ plane.

Fig. 9. Maximum available power in the wind and generator power.

Illustratively, the trajectory of the controlled system in the state space ($\sigma - \dot{\sigma}$ plane) is shown in Fig. 8.

The maximum available power in the wind, i.e., (1) with $\lambda = \lambda_{\text{opt}}$, and the generator power are plotted in Fig. 9. As the system successfully operates with $\lambda = \lambda_{\text{opt}}$ ($\sigma = 0$), the primary control objective is satisfactorily attained, and the generator power finely follows the maximum, except for the gusts and turbulence and an offset due to friction and other losses.

The electrical resistant torque of the generator $-T_e$ and the turbine torque are shown in Fig. 10 together with the unmodeled friction torque T_{fr}. A detail of the generator torque oscillations is shown in the zoomed image inside the figure. The small amplitude of these oscillations can be appreciated, showing the excellent behavior of the controlled system regarding mechanical loads.

The evolution of the control input $u(t) = |\cos(\alpha)|$ is depicted in Fig. 11. Note that its smoothness and, therefore, the smoothness of the physical control input α are responsible for the reduced mechanical stresses and, practically, the absence of chattering.

Finally, the electric variables of the WECS are depicted. The $d - q$ components of the stator and rotor currents and voltages can be seen in Figs. 12 and 13, respectively.
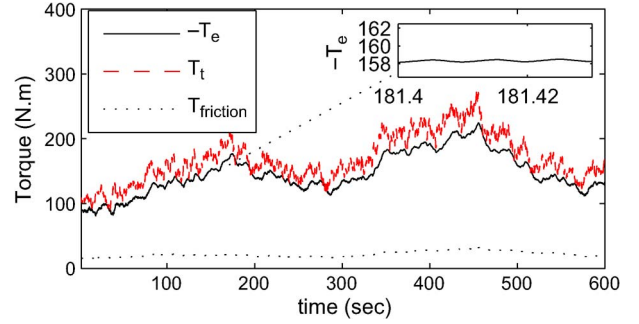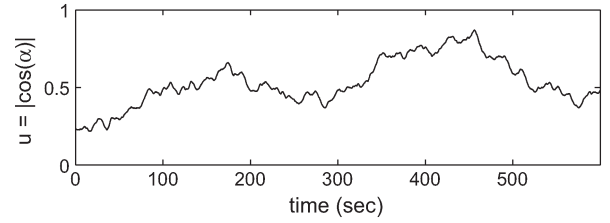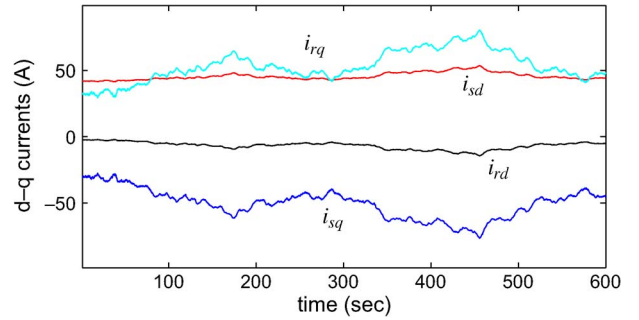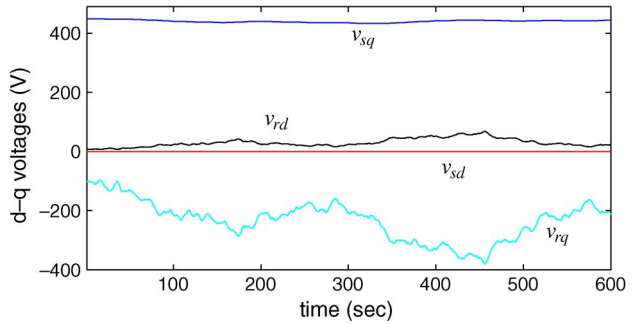

Fig. 10. Generator, turbine, and friction torques.

Fig. 11. Control action $u = |\cos(\alpha)|$.

Fig. 12. $d-q$ components of stator and rotor electrical currents.

Fig. 13. $d-q$ components of stator and rotor voltages.

B. Fixed-Gain ST and Comparison

The simulations for the WECS using the fixed-gain controller designed in Section III-B demonstrated the achievement of the main control objective of maximizing the captured power. The controller proved its robustness to the several disturbances and uncertainties already described, maintaining the chattering and mechanical stresses at low levels. Representative simulated results, corresponding to the wind profile displayed at the beginning of the section (see Fig. 5), are presented and discussed in the sequel, comparing them to the ones corresponding to the variable-gain controller.
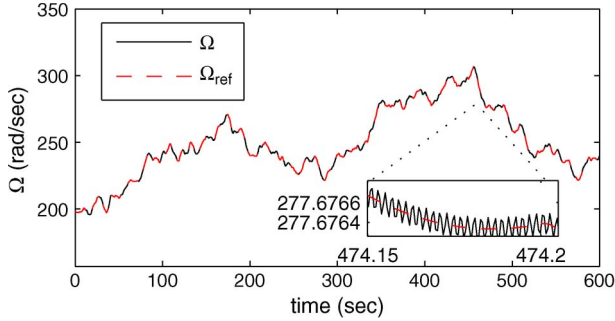
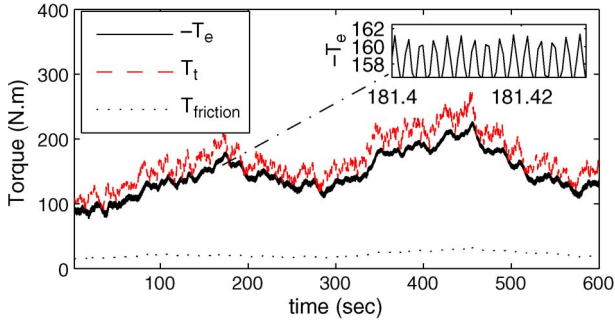Fig. 14.   Rotational speed and speed reference (fixed-gain ST).

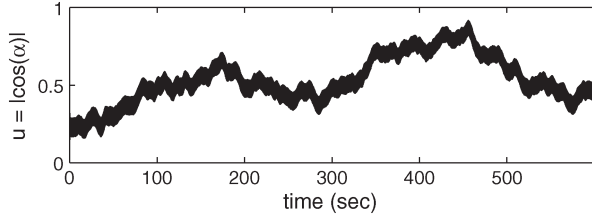Fig. 15.   Generator, turbine, and friction torques (fixed-gain ST).

Fig. 16.   Control action $u = |\cos(\alpha)|$ (fixed-gain ST).

The rotational speed and the reference Ω_{ref} are displayed together in Fig. 14. As in the case of the previous controller, the difference between both variables is negligible, consequently fulfilling the sliding condition. The oscillations shown in the zoom boxes of Figs. 6 and 14, which are directly related to the chattering, allow to mention that, although both cases exhibit an excellent tracking behavior in this regard, the variable-gain controller is better.

The time profiles of the electrical and the turbine torques, $-T_e$ and T_t, respectively, are depicted in Fig. 15. A look at its zoom box evidences the satisfactory mechanical behavior, existing oscillations which are kept below 4%. The comparison with the case of the variable-gain controller (see Fig. 10), where the variations of the generator torque are maintained smaller than 0.2%, shows the improvement obtained on this matter by having variable gains in the control action. Note that, from the standpoint of mechanical stress, the variations of the torque applied to the shaft are reduced by 20 times in the case of the variable-gain design, without significantly increasing the complexity of the control.

Finally, the time evolution of the control input $u(t) = |\cos(\alpha)|$ is presented in Fig. 16. When compared to the one corresponding to the variable-gain algorithm (see Fig. 11), the smoothness of the latter must be pointed out, it being responsible for the better mechanical behavior.

V. CONCLUSION

In this paper, an ST algorithm with variable gains was applied to the control of a variable-speed WECS with slip power recovery to maximize the energy extracted from the wind. A Lyapunov-based controller was designed considering a reduced model of the WECS and tested afterward through extensive simulations using a realistic full-order model, including several disturbances and uncertainties.

The design procedure required the finding of analytical expressions for certain functions to bind such disturbances and uncertainties. Those functions, together with five design parameters, were employed in the calculation of the variable gains of the controller. The find of the bounds and the overall controller tuning is not straightforward, but it is an offline procedure. On the other hand, the resultant WECS control algorithm is relatively simple; hence, the online computational cost is considerably low.

The proposed strategy proved to be suitable for this WECS application, showing a highly robust behavior at accurately tracking the maximum conversion efficiency, which is determined by the randomly varying wind speed. A special important feature of the control law synthesized following this ST approach is the smoothness of the converter firing angle, facilitating its realizability in commutated systems and allowing captured power maximization, very low mechanical stress, and practically no output chattering.

An additional controller based on the ST algorithm with fixed gains, also Lyapunov designed, was developed for the studied WECS. Simulations ran under conditions similar to the variable-gain case proved robust tracking behavior. Regarding chattering and mechanical fatigue, the controller has an acceptable performance. However, the improvement of the variable-gain ST controller must be pointed out in this matter.

APPENDIX

A. Nominal and Design Parameters

$P_{\mathrm{rated}} = 60$ kW; $\omega_s = 2\pi 50$ rad/s; $V_s = 460/\sqrt{3}$;
$\quad R_s = 119$ mΩ; $R_r = 238$ mΩ; $R_f = 25.9$ mΩ;
$\quad L_s = L_r = 1.4$ mH; $L_f = 10.1$ mH; $M_s = 35.1$ mH;
$\quad \rho = 1.2242$ Kg/m^3; $J = 7.0623$ Kgm^2; $R = 6.75$ m;
$\quad c_0 = -1.142\ 10^{-2}$; $c_1 = 2.214\ 10^{-4}$; $c_2 = -1.03\ 10^{-6}$;
$\quad c_3 = 1.191\ 10^{-9}$; $n_1 = n_2 = 1.2$; $p_p = 2$;
$\quad A_3 = 8.117$; $A_2 = 3.664$; $A_1 = 7.59$; $A_0 = 0.02$;
$\quad |\dot{\nu}_s| \leq 0.09$; $|\ddot{\nu}_s| \leq 0.07$; $\left|\nu_s^{(3)}\right| \leq 0.01$; $k_c = 0.072$;
$\quad \epsilon = 0.001$; $p_3 = 0.0069$; $p_2 = -0.002$; $p_1 = 0.00579$;
$\quad \delta_1 = 0.62$; $\delta_2 = 0.01$; $k_1 = 130$; $k_2 = 2.37$;
$\quad \delta = 0.0001$;

Rendering to the fast shaft side: $k_{\mathrm{gb}} = 19.85$, $T_t = T_{\mathrm{tlow}}/k_{\mathrm{gb}}$, $\Omega = \Omega_t k_{\mathrm{gb}}$, and $J = (J_t/k_{\mathrm{gb}}^2 + J_g)$, where J_t and J_g are the inertia of the turbine rotor and of the generator rotating parts, respectively.

B. Expression for $\tilde{G}(z_1, t)$

$$\tilde{G}(z_1, t)$$
$$= z_1^3 \frac{9n^2\pi R^6 V_s'^3 \rho}{2J^3\nu^2 R_b^3\Omega_s^2}\left(V_s'\nu R_b\Delta c_3 - 2c_3 V_s'\Delta R_b\nu\right.$$
$$\left. + c_3 R_b\left(V_s'\Delta\nu - 4\Delta V_s\nu\right)\right)$$

$$+ F(z_1, t) - F(0, t) + T_{\mathrm{fr}}(z_1, t) + z_1^2 \frac{3n\pi R^5 V_s' \rho}{2J^2 R_b^2 \Omega_s}$$

$$\times (c_2 (2\Delta V_s' R_b - V_s' \Delta R_b) - 3V_s' \Delta R_b c_3 \lambda_{\mathrm{opt}}$$

$$+ R_b (3\lambda_{\mathrm{opt}} (2\Delta V_s' c_3 + V_s' \Delta c_3) + V_s' \Delta c_2))$$

$$+ \frac{z_1}{2JR_b^2 \Omega_s^2} \left(6V_s'^2 \Delta R_b - 12V_s' \Delta V_s' R_b + \pi R^4 \rho R_b^2 \Omega_s^2 \right.$$

$$\times (\Delta\nu c_1 + \nu\Delta c_1 + \lambda_{\mathrm{opt}} (2\Delta\nu c_2 + 2\nu\Delta c_2)$$

$$\left. + 3\lambda_{\mathrm{opt}}^2 (\Delta\nu c_3 + \nu\Delta c_3)) \right)$$

$$- \lambda_{\mathrm{opt}} \frac{3V_s'^2 \Delta\nu + J\Delta R_b \Omega_s^2 \dot\nu}{3nRV_s'^2 \Omega_s}$$

$$+ \frac{\pi R^3 \nu\rho\Omega_s}{6nV_s'^3} \sum_{i=0}^{3} ((V_s' \Delta R_b \nu + 2R_b (V_s' \Delta\nu - \nu\Delta V_s')) c_i$$

$$+ V_s' \nu R_b \Delta c_i) \lambda_{\mathrm{opt}}^i$$

$$+ \frac{\lambda_{\mathrm{opt}} R_b J\Omega_s}{3nRV_s'} (2\Delta V_s' \dot\nu - V_s' \Delta\nu \ddot\nu)$$

C. Park Model

The nonlinear differential equations that describe the topology under study in a synchronously rotating direct quadrature $(d-q)$ frame are

$$\begin{bmatrix} 0 \\ V_s \\ -(V_s'')' u \sin(\varphi) \\ -(V_s'')' u \cos(\varphi) \end{bmatrix} = \mathbf{Z} \begin{bmatrix} i_{\mathrm{sd}} \\ i_{\mathrm{sq}} \\ i_{\mathrm{rd}}' \\ i_{\mathrm{rq}}' \end{bmatrix} \tag{40}$$

with

$$\mathbf{Z} = \begin{bmatrix} R_s + L_s p & -w_s L_s & M_s p & -\omega_s M_s \\ \omega_s L_s & R_s + L_s p & \omega_s M_s & M_s p \\ M_s p & -s\omega_s M_s & R_b' + L_b' p & -s\omega_s L_r' \\ s\omega_s M_s & M_s p & s\omega_s L_r' & R_b' + L_b' p \end{bmatrix}$$

where p is the time derivative operator, $\varphi = \tan^{-1}(i_{\mathrm{rd}}/i_{\mathrm{rq}})$, $L_b = L_r + 0.55L_f$, with L_r and L_f being the inductances of the rotor and dc link, respectively, and M_s is the magnetizing inductance. Quotation marks applied to V_s indicate that it has been referred to the inverter terminals by n_2. The equation for the generator torque, which replaces (5), is

$$T_e = p_p M_s \left(i_{\mathrm{sq}} i_{\mathrm{rd}}' - i_{\mathrm{sd}} i_{\mathrm{rq}}' \right) \tag{41}$$

where p_p corresponds to the number of pole pairs.

REFERENCES

[1] Global wind energy output 2010, Global Wind Energy Council. [Online]. Available: http://www.gwec.net

[2] World wind energy report 2010, World Wind Energy Assoc., Apr. 2011. [Online]. Available: http://www.wwindea.org/

[3] B. Beltran, T. Ahmed-Ali, and M. Benbouzid, "High-order sliding-mode control of variable-speed wind turbines," *IEEE Trans. Ind. Electron.*, vol. 56, no. 9, pp. 3314–3321, Sep. 2009.

[4] G. Bartolini, A. Ferrara, and E. Usai, "Chattering avoidance by second order sliding mode control," *IEEE Trans. Autom. Control*, vol. 43, no. 2, pp. 241–246, Feb. 1998.

[5] G. Bartolini, A. Levant, A. Pisano, and E. Usai, "2-sliding mode with adaptation," in *Proc. 7th IEEE Mediterranean Conf. Control Syst.*, Haifa, Israel, 1999.

[6] I. Boiko, L. Fridman, A. Pisano, and E. Usai, "Analysis of chattering in systems with second-order sliding modes," *IEEE Trans. Autom. Control*, vol. 52, no. 11, pp. 2085–2102, Nov. 2007.

[7] C. Edwards, E. Fossas Colet, and L. Fridman, Eds., *Advances in Variable Structure and Sliding Mode Control*. Berlin, Germany: Springer-Verlag, 2006.

[8] S. Emelyanov, S. Korovin, and A. Levant, "High-order sliding modes in control systems," *Comput. Math. Model.*, vol. 7, no. 3, pp. 294–318, 1996.

[9] L. Fridman and A. Levant, *Sliding Mode Control in Engineering*. New York: Marcel Dekker, 2002, ch. 3, pp. 53–101.

[10] J. Hung, W. Gao, and J. Hung, "Variable structure control: A survey," *IEEE Trans. Ind. Electron.*, vol. 40, no. 1, pp. 2–22, Feb. 1993.

[11] A. Levant, "Sliding order and sliding accuracy in sliding mode control," *Int. J. Control*, vol. 58, no. 6, pp. 1247–1263, 1993.

[12] A. Levant, "Principles of 2-sliding mode design," *Automatica*, vol. 43, no. 4, pp. 576–586, Apr. 2007.

[13] A. Sabanovic, L. M. Fridman, and S. Spurgeon, Eds., *Variable Structure Systems: From Principles to Implementation*. Stevenage, U.K.: IET, 2004.

[14] H. Shi, Y. Feng, and X. Yu, "High-order terminal sliding modes control for induction motor," in *Proc. 36th IEEE IECON*, Nov. 2010, pp. 2391–2395.

[15] Q. Ahmed and A. Bhatti, "Estimating SI engine efficiencies and parameters in second-order sliding modes," *IEEE Trans. Ind. Electron.*, vol. 58, no. 10, pp. 4837–4846, Oct. 2011.

[16] S. Benelghali, M. El Hachemi Benbouzid, J. Charpentier, T. Ahmed-Ali, and I. Munteanu, "Experimental validation of a marine current turbine simulator: Application to a permanent magnet synchronous generator-based system second-order sliding mode control," *IEEE Trans. Ind. Electron.*, vol. 58, no. 1, pp. 118–126, Jan. 2011.

[17] A. Dávila, J. Moreno, and L. Fridman, "Variable gains super-twisting algorithm: A Lyapunov based design," in *Proc. Amer. Control Conf.*, Baltimore, MD, Jun. 2010.

[18] J. A. Moreno and M. Osorio, "A Lyapunov approach to second-order sliding mode controllers and observers," in *Proc. 47th IEEE CDC*, Dec. 2008, pp. 2856–2861.

[19] J. Baroudi, V. Dinavahi, and A. Knight, "A review of power converter topologies for wind generators," *Renew. Energy*, vol. 32, no. 14, pp. 2369–2385, Nov. 2007.

[20] Z. Salameh and L. Kazda, "Analysis of the steady state performance of the double output induction generator," *IEEE Trans. Energy Convers.*, vol. EC-1, no. 1, pp. 26–32, Mar. 1986.

[21] R. Spée, S. Bhowmik, and J. Enslin, "Novel control strategies for variable-speed doubly fed power generation systems," *Renew. Energy*, vol. 6, no. 8, pp. 907–915, Nov. 1995.

[22] I. Munteanu, S. Bacha, A. Bratcu, J. Guiraud, and D. Roye, "Energy-reliability optimization of wind energy conversion systems by sliding mode control," *IEEE Trans. Energy Convers.*, vol. 23, no. 3, pp. 975–985, Sep. 2008.

[23] T. Burton, D. Sharpe, N. Jenkins, and E. Bossanyi, *Wind Energy Handbook*. Chichester, U.K.: Wiley, 2001.

[24] H. De Battista, P. Puleston, R. Mantz, and C. Christiansen, "Sliding mode control of wind energy systems with DOIG-power efficiency and torsional dynamics optimization," *IEEE Trans. Power Syst.*, vol. 15, no. 2, pp. 728–734, May 2000.

[25] V. Utkin, "Sliding mode control design principles and applications to electric drives," *IEEE Trans. Ind. Electron.*, vol. 40, no. 1, pp. 23–36, Feb. 1993.

[26] H. Khalil, *Nonlinear Systems*, 3rd ed. Upper Saddle River, NJ: Prentice-Hall, 2002.

[27] P. Puleston, R. Mantz, P. Battaiotto, and F. Valenciaga, "Sliding mode control for efficiency optimization of wind energy systems with double output induction generator," *Int. J. Energy Res.*, vol. 24, no. 1, pp. 77–92, Jan. 2000.

[28] F. D. Bianchi, H. de Battista, and R. Mantz, *Wind Turbine Control Systems: Principles, Modeling and Gain Scheduling Design*. London, U.K.: Springer-Verlag, 2007.

Authors' photographs and biographies not available at the time of publication.